Remote Sensing for Vital Information Based on Spectral-Domain Harmonic Signatures

YU RONG (iD), Student Member, IEEE
DANIEL W. BLISS, Fellow, IEEE
Arizona State University, Tempe, AZ, USA

In this paper, we propose an efficient and robust non-contact heart rate estimation algorithm. The key idea is to recover the fundamental heartbeat frequency from its higher-order spectral features. Our contributions are threefold: 1) carefully review and examine possible approaches in vital signs detection with ultra-wide band (UWB) impulse radar; 2) numerically and experimentally show an important result that, in the spectral domain, the fundamental heartbeat signal is respiration-interference-limited, whereas its higher-order harmonics are noise-limited; and 3) implement an adaptive heart rate monitoring algorithm based on the proposed theory, which is feasible with continuous monitoring. To justify the proposed theory, we perform a spectral analysis of the harmonics of vital signs signal. We validate the proposed algorithm using a controlled vital sign simulator. We experimentally demonstrate the effectiveness of the harmonics-based heart rate estimation algorithm and compare it against existing methods. For completeness, we also provide a limitation analysis of the proposed algorithm.

I. INTRODUCTION

Ultra-wide band (UWB) radar systems are very useful in homeland security, rescue missions, and obscured object detection applications. Different from other radar systems, the UWB radar system has strong penetrating ability compared to optical systems, and fine range resolving ability compared to continuous wave (CW) radar systems [1]–[3]. By using an impulse or frequency-modulated signal, UWB radars can measure micro-motion such as vital signs [4], human gait [5], and distinguish targets at different ranges, such as human counting application [6]. More popularly, UWB impulse radars employ a carrier-free signaling scheme and transmit a very narrow pulse, on the order of nanosecond, achieving a bandwidth of couple of GHz. Typically, for a UWB radar, the range is sampled at analog to digital converter (ADC) rate and cross range is sampled at the radar output frame repetition rate [7].

UWB radar can non-invasively monitor internal physiological motion of the organs of a body such as heartbeat, lung, and blood flooding, by transmitting low-energy electromagnetic waves, leading to transformational applications in medical diagnosis [4], [8], [9]. In this paper, we discuss monitoring vital signs of stationary human subjects remotely using a UWB impulse radar by coherently processing the time history of narrow pulses backscattered by the human chest. Detecting human vital sign using short-range radar technology is an important application in health development. The non-invasive detection of vital sign has led to several potential applications such as elderly care and in-hospital monitoring.

Recently, smart wearables, such as smart watches and headphones, for healthcare, have become available and convenient. Most of these devices use photoplethysmography sensor (often a green light LED sensor) to measure the intensity of light reflected through tissue to detect the pulse information. Compared with wearable technologies, the radar technology causes no discomfort to the human subject since no sensor is physically connected to the human body. In some situations, these wearables are difficult to use on infants or skin-burned patients. Another concern for smart wearables is power consumption. The light-based sensors consume much more energy than the radar sensors for vital signs monitoring. These vital signs radar sensors are generally portable, with low power consumption and low power emission, satisfying the federal communications commission (FCC) Part 15 requirement.

This paper is organized as follows. In Section II, we introduce related works on radar-based vital sign detection and the main motivation for this paper. In Section III, we present the UWB impulse radar signal model for extracting vital information. In Sections III-A and III-B, we examine different approaches for vital sign detection in great detail. In Section IV, we preset the proposed theory and provide theoretical justification. Accordingly, in Section IV-D, we propose a harmonics-aided heart rate estimation algorithm. In Section V, we provide extensive experimental examples to demonstrate the proposed theory and algorithm. Finally,

in Section VI, we conclude the paper and identify on-going efforts.

II. BACKGROUND

Theoretical analysis for vital sign extraction has been well-established for CW radar. Single channel selection selects either the I channel or the Q channel is selected for vital signs detection. This method, however, suffers when the signal sensitivity is very weak in I or Q channels. To deal with this problem, a complex signal demodulation (CSD) method was proposed in [10]. A theoretical analysis on spectrum representation is carried out, demonstrating that ideally the Fourier spectrum of the vital signs is actually a pulse train with decaying amplitudes associated with each pulse. This is an important result because it states that the fundamental heartbeat frequency is closely spaced with the higher-order harmonics (usually the third) of the fundamental respiration frequency and often these higher-order harmonics are much stronger than the heartbeat signal strength. Because of these two facts, long-term heart rate monitoring using CSD is not possible. A phase-based method, called Arctangent demodulation (AD) method, was proposed in [11] with phase calibration techniques. Similar phase-based methods and extension of AD method was reported in [12].

On the other hand, the possibility of vital signs extraction using UWB impulse radar was reported in [13]–[15]. However, a detailed discussion and theoretical justification on the feasibility of applying the popular CSD method and AD method for UWB impulse radar is not available. A limited discussion on this subject was carried out in [16]. Due to different signaling schemes, the mathematical formulation of UWB impulse radar for vital sign detection is somewhat different from that of the CW radar. Besides, we show that the CSD and AD methods and related methods can be applied for vital sign detection using a UWB impulse radar.

In this paper, we highlight an important result: spectrally, the fundamental heartbeat frequency is respiration-interference-limited, whereas its higher-order harmonics are noise-limited. These higher-order statistics related to heartbeat can be a robust indication when the fundamental heartbeat is masked by the strong lower-order harmonics of respiration and when phase calibration is not accurate if phase-based method is used. Additionally, we propose a novel approach based on the concept of harmonics-based heart rate estimation. This approach was demonstrated in [17] and [18] for multiple-subject heart rates detection. In this paper, we elaborate this concept and propose an adaptive heart rate estimation algorithm. We also provide more theoretical analysis and experimental examples. A high-level signal processing chain for the heart rate estimation based on its higher-order harmonics is illustrated in Fig. 1.

Our contributions:

1) review and compare existing vital signs detection for impulsed-based UWB radar;
2) numerically and experimentally show an important result that, in the spectral domain, the fundamental heartbeat signal is respiration-interference-

limited, whereas its higher-order harmonics are noise-limited;
3) present and implement an adaptive heart rate estimation algorithm using multiple heartbeat related spectral features.

III. VITAL SIGN MODELING IN UWB IMPULSE RADAR

In this section, we discuss the signal model for vital sign detection using a UWB impulse radar. We summarized and extended the results in [13] and [14]. The received signal was directly sampled in radio frequency (RF) and then digitally converted to the complex baseband. In our model, τ denotes the fast sampling time and ν is the transformed frequency component, whereas t denotes the slow cross-range sampling time and f denotes the corresponding Fourier domain component. The vital signs of a subject at a nominal distance d_0 can be modeled a sum of two periodic signals from respiratory and cardiac activities

$$d(t) = d_0 + M_b \sin(2\pi f_b t) + M_h \sin(2\pi f_h t) \quad (1)$$

where M_b is the amplitude of respiratory activity, and M_h is the amplitude of cardiac activity. f_b and f_h are respiration and heartbeat frequencies. The received signal can be modeled as a sum of the target response and the delayed, attenuated versions of the transmitted pulse due to static environment

$$r(t, \tau) = A_T p(\tau - \tau_D(t)) + \sum_i A_i p(\tau - \tau_i) \quad (2)$$

where $p(t, \tau)$ is the generated short pulse, centered at the carrier frequency F_c. A_T and A_i denote the magnitude of the target response and the multi-path components, whereas $\tau_D(t) = 2d(t)/c$ and τ_i are the corresponding delays, where c is the speed of light. The signal of interest can be modeled as

$$r_0(t, \tau) = A_T p(\tau - \tau_D(t)) \quad (3)$$

where the multi-path components due to static environment can be eliminated by mean subtraction. The received signal is then down converted to the complex baseband and represented as

$$\begin{aligned} y(t, \tau) &= r_0(t, \tau) e^{-j2\pi F_c \tau} \\ &= A_T p(\tau - \tau_D(t)) e^{-j2\pi F_c \tau}. \end{aligned} \quad (4)$$

A. I/Q Channel-Based Approaches

In this section, we show that the CSD method using I/Q channels for vital sign detection can be applied to the complex baseband signal [see (4)]. The CSD method can be performed directly onto (4). By invoking the two-dimensional (2-D) Fourier transform, we derive the final expression for the Fourier transform of the complex baseband signal in slow time

$$Y(f, \tau) = A_T e^{-j2\pi F_c \tau_0}$$
$$\times \sum_{k=-\infty}^{\infty} \sum_{l=-\infty}^{\infty} C_{k,l}(\tau) \delta(f - kf_b - lf_h) \quad (5)$$
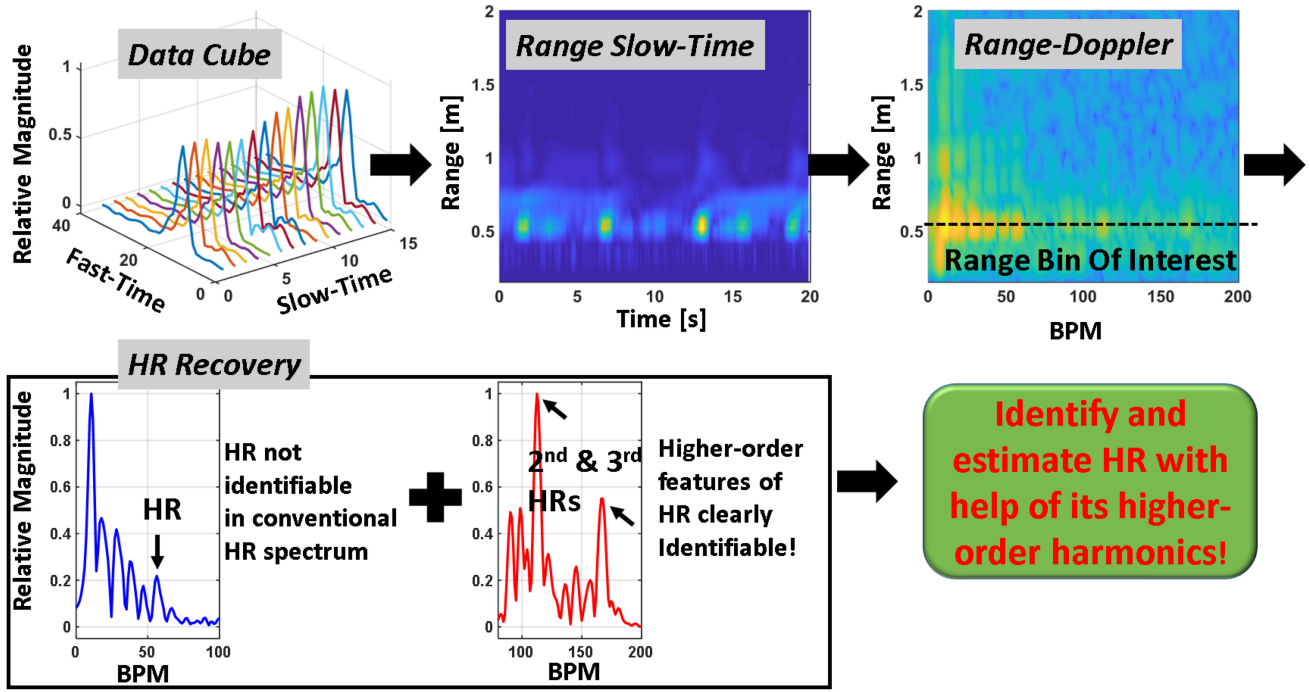
Fig. 1. High-level processing diagram: recover the fundamental heartbeat frequency from its higher-order harmonics.

$$|Y(f, \tau)| \leq |A_T| \sum_{k=-\infty}^{\infty} \sum_{l=-\infty}^{\infty} |C_{k,l}(\tau_0)| \tag{6}$$
$$\times \delta(f - kf_b - lf_h) = |Y(f, \tau_0)|$$

where $C_{k,l}(\tau) = \int d\nu [P(\nu + F_c)e^{j2\pi \nu(\tau - \tau_0)} J_k(4\pi(\nu + F_c) m_b/c) J_l(4\pi(\nu + F_c) m_h/c)]$ and $C_{k,l}$ achieves a maximum value of $C_{k,l}(\tau_0)$ at τ_0. $P(\nu + F_c)$ is the fast-time Fourier transform of the transmitted pulse shifted to dc.

B. Phase-Based Approaches

In this section, we show how to extract phase variation due to vital sign activity. The fast-time (ν) Fourier transform is applied to (4) to separate out the time delay in $p(\tau - \tau_D(t))$

$$Y(t, \nu) = A_T P(\nu + F_c)e^{-j2\pi(\nu + F_c)\tau_D(t)}. \tag{7}$$

In order to evaluate the above equation, one can set $\nu = 0$, corresponding to the fast-time Fourier transform evaluated at dc as suggested in [14]

$$Y(t, 0) = A_T P(F_c)e^{-j2\pi F_c \tau_D(t)}. \tag{8}$$

For convenience, (8) is re-written as

$$Y(t, 0) = A_T P(t, F_c)e^{-j2\pi F_c \tau_D(t)}$$
$$= A_T \left(\int_{-\infty}^{\infty} d\tau p(t, \tau)e^{-j2\pi F_c \tau} \right) \tag{9}$$
$$\times e^{-j2\pi F_c \tau_D(t)}$$

where $P(t, Fc)$ is a constant complex value since the transmitted pulse $p(t, \tau)$ is constant over slow time. $P(t, Fc)$ is thus decomposed as $M_p e^{-j\phi_P}$ with magnitude M_P and

phase ϕ_P

$$Y(t, 0) = A_T M_P e^{-j(2\pi F_c \tau_D(t) + \phi_P)}. \tag{10}$$

Note that A_T and M_P are real numbers and the vital information is preserved in the phase term. The I and Q channels can be represented as

$$I(t) = A_T M_P \cos(2\pi F_c \tau_D(t) + \phi_P) \tag{11}$$
$$Q(t) = A_T M_P \sin(2\pi F_c \tau_D(t) + \phi_P). \tag{12}$$

1) *Phase Demodulation Methods:* One way to reliably detect vital information in a quadrature demodulation system is to use the AD method. By directly calculating the phase shift as an Arctangent function of $Q(t)/I(t)$, accurate phase variation extraction is possible. The phase variation is linearly related to the vital signs as follows:

$$\Phi(t) = \text{unwrapping} \left\{ \text{atan}\left(\frac{Q(t)}{I(t)} \right) \right\}$$
$$= \frac{4\pi M_b \sin(2\pi f_b t)}{\lambda} + \frac{4\pi M_h \sin(2\pi f_h t)}{\lambda}$$
$$+ \frac{4\pi d_0}{c} + \phi_P \tag{13}$$
$$= \frac{4\pi M_b \sin(2\pi f_b t)}{\lambda} + \frac{4\pi M_h \sin(2\pi f_h t)}{\lambda}$$
$$+ \phi_{\text{DC}}$$

where $\lambda = F_c/c$ is the wavelength and $\phi_{\text{DC}} = 4\pi d_0/c + \phi_P$ denotes the total dc information including two phase terms: the first term $4\pi d_0/c$ is determined by the target position information and the second term is determined by the transmitted pulse waveform and the center frequency. Often a phase unwrapping function is needed to deal with

the phase discontinuity outside of $[-\pi/2, \pi/2]$ due to the Arctangent function. The result in (13) is the ideal situation. In general, phase noise is inevitable and independently present in I/Q channels ε_I and ε_Q. Let us define the overall vital sign as $V(t) = M_b \sin(2\pi f_b t) + M_h \sin(2\pi f_h t)$. The complete signal model that captures this I/Q imbalance effect is given as follows:

$$\dot{\Phi}(t) = \text{unwrapping} \left\{ \text{atan} \left(\frac{\dot{Q}(t)}{\dot{I}(t)} \right) \right\}$$

$$= \text{unwrapping} \tag{14}$$

$$\left\{ \text{atan} \left(\frac{A_Q \sin(4\pi V(t)/\lambda + \varphi_Q) + \mathcal{D}_Q}{A_I \cos(4\pi V(t)/\lambda + \varphi_I) + \mathcal{D}_I} \right) \right\}$$

where A_i, φ_i and $\mathcal{D}_i$, $i = I$, or Q, represent amplitude imbalance, phase imbalance, and dc offset. The total residual phase in I/Q channels contain two parts: dc and phase noise, $\mathcal{D}_I = \phi_{\text{DC}} + \varepsilon_I$ and $\mathcal{D}_Q = \phi_{\text{DC}} + \varepsilon_Q$. For our case, the raw radar data are directly RF sampled and the downconversion is done in digital signal processor (DSP). Therefore, there are no amplitude and phase imbalances, and $A_I = A_Q = A_0$ and $\varphi_I = \varphi_Q = \varphi_0$. Only dc offsets in I/Q channels need to be compensated. If perfect correction is done, (14) is reduced to

$$\dot{\Phi}(t) = \text{unwrapping}$$

$$\left\{ \text{atan} \left(\frac{A_0 \sin(4\pi V(t)/\lambda + \varphi_0)}{A_0 \cos(4\pi V(t)/\lambda + \varphi_0)} \right) \right\}$$

$$= \frac{4\pi V(t)}{\lambda} + \varphi_0 \tag{15}$$

$$= \frac{4\pi M_b \sin(2\pi f_b t)}{\lambda} + \frac{4\pi M_h \sin(2\pi f_h t)}{\lambda} + \varphi_0.$$

Now the Fourier transform can be directly applied to the extracted phase in (15). Two peaks in the spectrum domain correspond to the respiration frequency and the heartbeat frequency. Since φ_0 has no effect on the vital sign detection, it can be ignored.

2) Related Methods: Besides the AD method, the Logarithmic method [19] uses a similar approach to extract the phase variation that is directly related to the physiological motion. Alternatively, an extended differentiate and cross-multiply (DACM) method [12] can be used for vital sign detection. This method consists of two operations: differentiation and integration. The phase unwrapping is not required in DACM but phase calibration is required before applying the extended DACM method. The extended DACM can be treated as an alternative to other phase-based methods: the AD and the Logarithmic methods, since it only uses a different phase unwrapping method. The goal of phase-based methods is to suppress the inferencing harmonics, which is determined by the phase calibration process.

3) Phase Calibration Technique: A key process common to all phase-based approaches is phase calibration, which determines the heartbeat detection performance. The signal model in (15) is adopted and only dc offsets in the I/Q channels need to be compensated. This calibration process is often referred as circle fitting [20] or center tracking [21].

Note that if the RF to baseband conversion is done in the hardware, in which there are two independent I/Q receiver chains, the model in (14) should be considered and the corresponding phase calibration procedure is an elliptical fitting problem [22].

In this paper, we consider an iterative least-square fitting algorithm, called the Levenberg–Marquardt (LM) method [20]. It can effectively solve the least-squares problem with the following form, given n data points $(I(i), Q(i))$, $1 \leq i \leq n$

$$\mathcal{F} = \sum_{i=1}^{n} \left(\sqrt{(I(i) - \mathcal{D}_I)^2 + (Q(i) - \mathcal{D}_Q)^2} - \mathcal{R} \right)^2$$

$$= \sum_{i=1}^{n} d_i^2 \tag{16}$$

where $\mathcal{F}$ denotes the objective function. The geometric fit tries to minimize the mean square distance from the fitting circle to the distorted data points and produces a tuple of $(\mathcal{D}_I, \mathcal{D}_Q, \mathcal{R})$, where $\mathcal{D}_I, \mathcal{D}_Q$ are the center points and $\mathcal{R}$ is the radius of the fitting circle

$$\mathcal{R}^2 = (I(i) - \mathcal{D}_I)^2 + (I(i) - \mathcal{D}_Q)^2. \tag{17}$$

The efficiency and accuracy of the LM circle fitting method has been reported in many papers. A theoretical analysis of LM method was presented in [20]. A comparative study of dc offset calibration algorithms using the Doppler radar was presented in [23] and their result shows that the LM is one of the most accurate circle fitting algorithms. A representative experimental example is illustrated in Fig. 2. The dc corrected I/Q data samples are shown in Fig. 2(a) and an empirical convergence rate of LM method is shown in Fig. 2(b).

IV. OUR APPROACH

A. Heartbeat Spectral Harmonics Estimation

In this section, we present an effective heart rate estimation algorithm based on recovering the fundamental heartbeat frequency from its second-order harmonic. The main idea of this algorithm is shown in Fig. 3. This typical vital signs spectrum is obtained following the flow chart in Fig. 1. The detection range of the UWB radar is set to 1 m with a frame rate of 10 Hz. A 20-s moving processing window is used. In total, 200 frames of data are processed each time. The direct sampled RF signal is first acquired, then converted to the complex baseband using the known radar parameters. The baseband signal is often organized in 2-D matrix format, one dimension representing fast-time samples (range profile) and the other representing the slow-time samples (vital motion of interest). The clutter mitigation is realized by mean subtraction. The range-Doppler matrix is obtained by applying Fourier transform on each range bin over time. The vital signs spectrum in Fig. 3 is one slice of the range-Doppler matrix at the selected range bin. In general, most of the respiratory and heartbeat activities happen in a single range bin and thus only the range bin with maximum spectral energy is used. Next, a bandpass
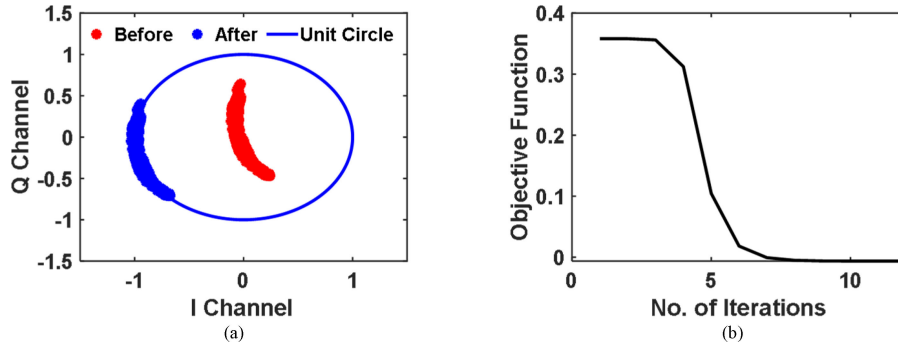
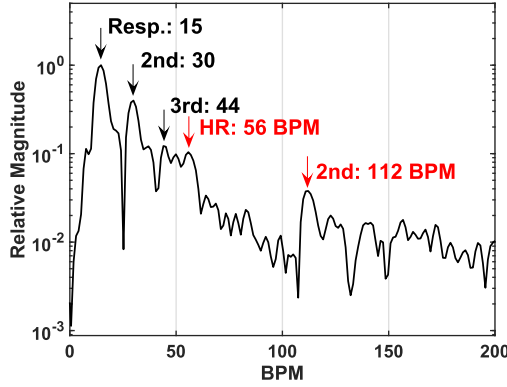Fig. 2. (a) I and Q data before and after dc calibration. (b) Empirical convergence rate of LM algorithm.

Fig. 3. Harmonics-based heart rate estimation.

filter is applied to emphasize the second-order harmonic of the heartbeat with negligible respiration harmonics. Once the second-order harmonic of the heartbeat frequency, f_{2nd}, is identified, the fundamental heartbeat frequency, or heart rate, can be recovered accordingly, $f_h = f_{2nd}/2$. A numerical justification of the proposed method is provided in next section.

B. Advantages: Free of Respiration Harmonics

Phase-based methods (AD) and its variations have been proposed to suppress respiration harmonics and inter-modulations. Theoretically, these algorithms can successfully eliminate respiration harmonics and inter-modulations. Their performance, however, are not guaranteed as demonstrated in [12] since the required phase calibration can never be perfect in a real system.

Instead of separating the fundamental heartbeat frequency from strong respiration harmonics and related inter-modulations in the relatively low frequency domain, the proposed method focuses in the relatively high frequency region and tries to locate the 2nd-order harmonic of the fundamental heartbeat frequency. In this way, the fundamental heartbeat frequency can be easily recovered. In this frequency region, the second-order harmonic of the heartbeat will compete with higher-order harmonics of respiration, e.g., the eighth respiration harmonics, or higher-order harmonics of inter-modulations. As the order number increases, the harmonic strength decreases dramatically. The

second-order harmonic of the heartbeat can thus be easily identified as if there is no interference from the respiration harmonics.

To further validate the theory, a quantitative analysis of the harmonics strength in the spectral domain is provided based on the complex baseband signal model in (6). Ignoring the common terms, the relative absolute magnitude of each frequency harmonic in $\delta(f - kf_b - lf_h)$ is determined by $C_{k,l}(\tau_0)$. A coarse representation of the harmonic strength of interest can be done based on $C_{k,l}(\tau_0)$ in (6)

$$
\begin{aligned}
C_{k,l}(\tau_0) &= \int_{-\mathrm{BW}/2}^{\mathrm{BW}/2} d\nu \, P(\nu + F_c) J_k\left(\frac{4\pi(\nu + F_c)M_b}{c}\right) \\
&\quad \times J_l\left(\frac{4\pi(\nu + F_c)M_h}{c}\right) \qquad (18) \\
&= \int_{-\mathrm{BW}/2+F_c}^{\mathrm{BW}/2+F_c} d\nu \, P(\nu) J_k\left(\frac{4\pi \nu M_b}{c}\right) J_l\left(\frac{4\pi \nu M_h}{c}\right) \\
&\approx \mathrm{BW} P(F_c) J_k\left(\frac{4\pi F_c M_b}{c}\right) J_l\left(\frac{4\pi F_c M_h}{c}\right),
\end{aligned}
$$
$$(19)$$

where BW denotes the system bandwidth, and change of variable and mean value approximation have been invoked to derive (19).

For clarity, we first compare the strength of the respiration harmonics to that of the heartbeat harmonics up to the second order. Then, we compare the higher-order inter-modulations to the heartbeat harmonics of interest. The normal resting breathing rate for an adult is about 12 to 20 beats per minute (B/Min) and the heart rate is about 60 to 80 on average [24]. For the numerical analysis, the breathing rate is set to 15 B/Min and the heart rate is set to 70 B/Min. In this case, the second-order harmonics of heartbeat (140 B/Min) is competing against the eighth, ninth, and tenth order harmonics of the respiration, ranging from 120 to 150 B/Min. Here, only the higher-order harmonics that are close to the second-order harmonics of the heartbeat are considered, otherwise they can be easily filtered out. The spectral magnitudes of the harmonics of interest are compared in Fig. 4 as a function of chest displacement (respiration) from 0.5 to 5.5 mm with a fixed heartbeat amplitude 0.08 mm [13], [25]. For normal respiratory activities, the second-order harmonic of the heartbeat is much
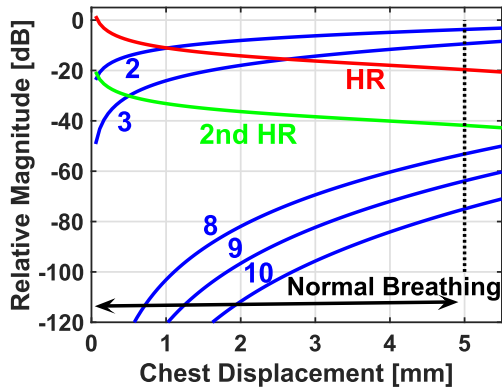
Fig. 4. Relative harmonic strength as a function of chest movement normalized with respect to the fundamental respiration. The blue curves and the single digits represent the respiration harmonics and the harmonic orders.
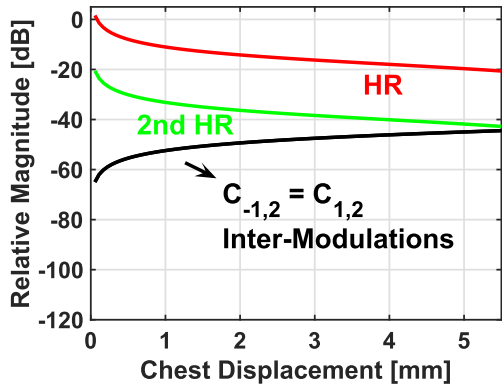

Fig. 5. Relative inter-modulation strength as a function of chest movement normalized with respect to the fundamental respiration.
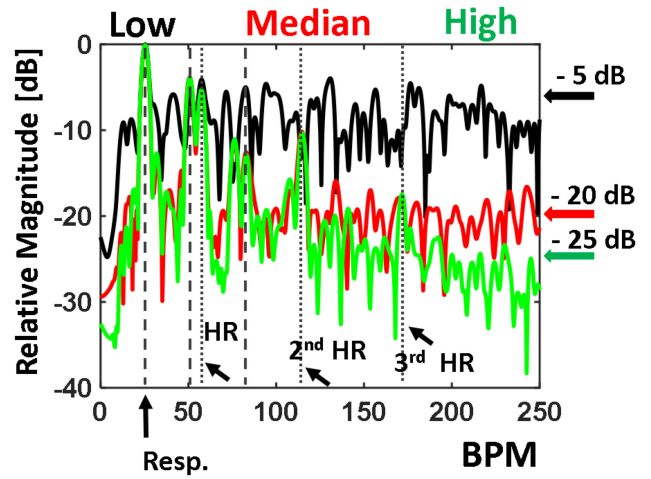

Fig. 6. Coherent processing gains from different pulse integration levels: low (black curve), median (red curve), and high (green curve); pre-defined heart rate: 56 B/Min, respiration rate: 26 B/Min. The dashed and dotted vertical lines denote the reference respiration harmonics and the heartbeat harmonics.
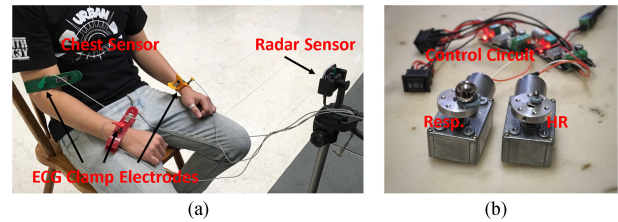

Fig. 7. Two experimental scenarios: (a) human subject; (b) controlled motorized vital sign simulator.

stronger than those of the higher-order harmonics of respiration (eighth, ninth, tenth). For different chest displacement, the fundamental heartbeat experiences interference from the lower-order harmonics of respiration (second). It should be noted that in general, higher-order harmonics with order number $m = k + l \geq 4$, where k and l are from $C_{k,l}(\tau_0)$, cannot be easily observed because of the weak vital sign motion and the background noise. The main challenge of monitoring fundamental heartbeat continuously is due to the spurious spectrum peaks such as second- or third-order harmonics of respiration. Fortunately, they are spectrally further away from the second-order harmonics of the heartbeat frequency. Therefore, it makes locating the heartbeat harmonics a respiration-interference free task.

Similarly, we compare the strength of the higher-order inter-modulations against the strength of the second-order harmonics of the heartbeat signal in Fig. 5. The associated inter-modulations close to 140 B/Min are $C_{k=-1,l=2}^{B}(\tau_0)$ and $C_{k=1,l=2}^{B}(\tau_0)$. Only the order numbers of inter-modulations $m \leq 3$ are considered.

C. Limitation Analysis

We have demonstrated the feasibility analysis of recovering the fundamental heartbeat frequency with the aid of its second-order harmonics in the spectral domain. In this section, we identify a few limitations for continuous heart rate monitoring for stationary subjects using the novel harmonics-based approach. Sufficient signal-to-noise-ratio (SNR) is required in order to detect the second-order harmonics of the heartbeat signal. The spectral energy of the heartbeat signal is about 20 dB lower than that of respiration. One would expect heartbeat harmonics to be even weaker. The tracking performance is very sensitive to background noise and random body motion. This method, therefore, fails when the test subject is seated further away, or facing the radar sideways, or wearing thick clothes. In our experiment, all the test subjects are asked to sit about 40 to 80 cm away from the radar, and keep still.

An important result that spectrally fundamental heartbeat is respiration-interference-limited, whereas its associated higher-order harmonics are noise-limited is presented earlier in this paper. In order to boost the vital signs SNR, the output frame rate of the radar is set as low as 10 Hz. The maximum radar pulse rate is about 40 MHz and the processing gain is achieved by coherently combining the pules. Here, we use a carefully designed example to demonstrate received signal SNR improvement from different integration levels. The following results in Fig. 6 are generated using a controlled motorized vital signs simulator as shown in Fig. 7(b). The respiration rate and the heart rate is

pre-defined for demonstration. As shown in Fig. 6, the received signal noise floor is significantly improved. By doing so, the higher-order harmonics such as second and third are clearly revealed and are easily isolated. On the contrary, the fundamental heartbeat frequency is competing against the closely located second-order harmonics of respiration and, therefore, is very difficult to correctly estimate using conventional methods.

D. Harmonics-Aided Heart Rate Estimation Algorithm

1) *Heartbeat Harmonics Filter Design:* In this section, we propose to adaptively utilize the fundamental heartbeat and its associated harmonics to make continuous measurement possible. Sine recovering the fundamental heartbeat frequency from its second-order harmonics or even third-order harmonics might not work when the SNR is low and the spectrum is noisy, two heart rate harmonic filters are designed. The primary filter γ is to filter out the spectrum content for the second- or third-order heartbeat harmonics and, therefore, estimate its frequency f_{HCS}. The secondary filter η is to estimate the fundamental heartbeat frequency $f_{1\text{st}}$. Only the lower cutoff frequencies need to be determined, whereas the upper cutoff frequencies are trivial. According to the resting adult heart rate statistics in Section IV-B, the frequency limits of the two harmonics filters are determined as

$$\gamma, \text{filter range} : 1.5 \leq f \leq 4 \text{ Hz}$$
$$\eta, \text{filter range} : 0.7 \leq f \leq 1.4 \text{ Hz}. \quad (20)$$

Thus, in addition to recovering the heartbeat frequency from its harmonics, the secondary filter η provides a second way to estimate the heartbeat frequency. The goal is to selectively combine different sources of frequency estimates and generate more robust estimates, so that continuous monitoring is possible.

2) *Spectral Peak Selection Criterion:* To further improve the robustness of our heart rate estimation algorithm, two efficient processing steps are proposed. First, full frequency spectrums are used for spectral peak localization since the I and Q data are used for a spectral analysis. That is because the spectral peaks might be either present in the negative spectrum or the positive portion. Second, when two spectral peaks with similar absolute frequency locations are present in the positive and negative spectrums, the selection is based on a new criterion, called peak to noise level (P2NL), instead of solely relying on the peak height

$$\text{P2NL} = \frac{\sum_{i=\text{pos}-2}^{\text{pos}+2} V_i}{\sum_{j=\text{pos}-50}^{\text{pos}+50} V_j} \quad (21)$$

where V_{pos} is the peak spectral value at posth position. The numerator is sum of the peak value and two nearby data samples to the right and to the left, totaling five data samples. The denominator is the sum of the corresponding 101 data values including the peak values and the noise-like data values. Based on this criterion, one of the two competing peaks with a larger P2NL value is selected. A more noise-robust peak spectrum gives a larger P2NL value.

3) *Adaptive Heart Rate Selection:* In this section, we present an adaptive heart rate selection scheme by summarizing the results presented in previous sections. The real-time signal processing algorithm starts when there are 200 frames ready, but the algorithm starts outputting the heart rate reading only if the frequency estimate of the second-order harmonic of the heartbeat is stable for 1 s, meaning that the heart rate estimate $f_h = f_{\text{HCS}}/2$ is stable for ten consecutive estimates and the variation is less than three beats. These estimates are obtained by applying the primary bandpass filter γ by selecting the peak location based on the P2NL criterion in (21). The purpose of waiting for stable estimates is to make sure the spectral peak is heartbeat harmonics not some random peaks. As demonstrated in Section IV-B, a stable spectral peak in the second-harmonics frequency region is the result of the cardiac activity with a high probability.

Similarly, the secondary heart rate estimate is obtained using the filter η. These estimates are stored along with the primary estimates from γ. However, they are only checked when the primary estimate start fluctuating wildly, such that the difference between the current estimate at time instance t, where t denotes some discrete sample index, and the previous output heart rate at time instance $t-1$ is larger than three beats, such as $|f_h^{t-1} - f_{\text{HCS}}^t/2| > 3$ and $|f_h^{t-1} - f_{\text{HCS}}^t/3| > 3$. Here, two situations are considered. The dominant spectral peak location f_{HCS} can be either the second-order harmonic of the heartbeat or occasionally the third-order harmonic. If the current estimates $f_{\text{HCS}}^t/2$ and $f_{\text{HCS}}^t/3$ are different from the previous heart rate estimate f_h^{t-1} by more than three beats, then the secondary estimate is compared against the previous output heart rate f_h^{t-1}. The secondary estimate is used when the difference is small such as $|f_h^{t-1} - f_{1\text{st}}^t| \leq 3$ and thus is chosen as the current output heart rate $f_h^t = f_{1\text{st}}^t$. Otherwise, both the current primary and the secondary estimates are ignored. The algorithm stops and print out warning message "Possible unreliable estimate due to body movement!".

Above procedures are repeated every time when a new data frame comes in until the recording time is reached. The proposed adaptive heart rate selection scheme is summarized in Table I.

V. RESULT DISCUSSION

In this section, we provide extensive examples to validate the proposed theory and the proposed heart rate estimation algorithm. The UWB impulse radar sensor is the Xethru X4M03 development kit.[*] The detailed hardware design can be found in [26]. For performance demonstration, we consider the time-frequency (2-D) analysis since we are observing a time-varying process, in addition to the conventional spectral (one-dimensional) analysis. Two experimental scenarios are considered: controlled motorized

---

[*]https://www.xethru.com/shop/x4m03-development-kit.html

TABLE I
Adaptive HR Selection Scheme

Moving processing window 20-s, with 1 sample increment each time
$t = t_0 \rightarrow$ **Start** processing when 200 frames of data is available
$\vdots$
$t = t_1 \rightarrow$ **Output** the first HR reading $f_h = f_{\text{HCS}}/2$ if f_{HCS} is stable for 1-s or 10 consecutive estimates
$\vdots$
$t = t_2 \rightarrow$ **Check** the difference between the current f_{HCS} and the previous f_h if $\|f_h - f_{\text{HCS}}/2\| \leq 3$, then output $f_h = f_{\text{HCS}}/2$ else check if f_{HCS} is close to the 3rd HR if $\|f_h - f_{\text{HCS}}/3\| \leq 3$ then output $f_h = f_{\text{HCS}}/3$ else check the secondary estimate if $\|f_h - f_{1\text{st}}\| \leq 3$ then output $f_h = f_{1\text{st}}$ else print out warning message and stop algorithm end end end
$\vdots$
$t = t_3 \rightarrow$ **Repeat** previous procedure until reach the recording time

TABLE II
System Parameters

Specification	Values
Center frequency	7.29 GHz
Bandwidth	1.4 GHz
Fast-time (RF) sampling rate	23.328 GHz
Slow-time sampling rate after coherent combing	10 Hz
Coherent processing time	20 s

Fig. 8. Overall spectral analysis: (b) controlled motorized vital sign simulator. Pre-defined heart rate: 58 B/Min, respiration rate: 26 B/Min; (b) human subject, ECG reference heart rate: 61 B/Min, respiration reference: 16 B/Min. The labeled numbers in above plots are rounded.

vital signs simulator and human subjects. The experimental setup is displayed in Fig. 7. Additionally, we demonstrate the accuracy of the proposed heart rate estimation algorithm by comparing against the reference pulse signal. What is more, we conduct a limitation test by showing that how the proposed method behaves in unfavorable situations in Fig. 11. Some of the key radar parameters are summarized in Table II.

A. Vital Sign Extraction

We validate our results with experimental examples from 1) vital signs simulator and 2) human subject. The results are generated from a 20-s data set. The conventional spectral analysis is conducted by comparing CSD, AD, and the proposed method.

Results from the controlled vital sign simulator are shown in Fig. 8(a). The motorized circulating frequencies are set to 26 and 58 B/Min corresponding to the respiration rate and heart rate, respectively. In this representative example, we can see that all the methods are able to identify the respiration frequency and the heartbeat frequency. However, the phase-based method suppresses the respiration
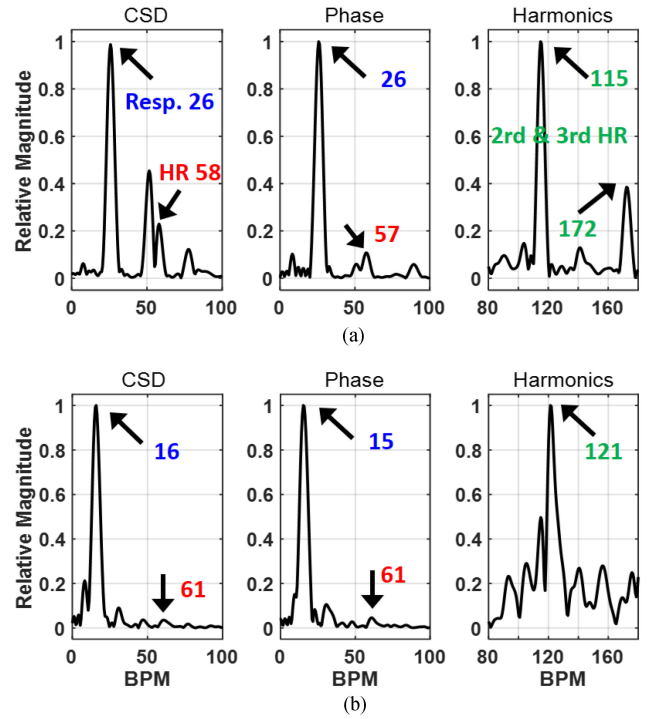
harmonics significantly and provides better identifiability for the heartbeat. For the proposed approach, at the heartbeat harmonics frequency region, the second-order harmonic is very distinct as if there is no interference from the respiration. Results from human subject are illustrated in Fig. 8(b). Similar results observed here. Vital signs are identified from all three methods. In the CSD spectrum, the heartbeat frequency can be identified with the help of an external reference pulse signal. There is a potential heartbeat spectral peak present at 61 B/Min, which is consistent with the reference. However, it is very hard to separate it out from the third-order respiration harmonic since it is competing against the nearby third-order respiration harmonic; although the phase-based method effectively suppresses the nearby spectrum and improves the heartbeat detection performance compared to that of CSD. Best performance in terms of identifiability is observed in the proposed method since the second-order heartbeat spectrum peak is easily identified and, therefore, correctly estimated.

B. Time-Frequency Analysis of Popular Heart Rate Estimation Algorithms

We compare popular heart rate estimation algorithms using waterfall plots, a time-frequency (2-D) representation. The following results are generated from a 60-s data set with a 20-s processing window and one sample increment each processing time. Again, we first show results from the controlled environment and then the human subject.
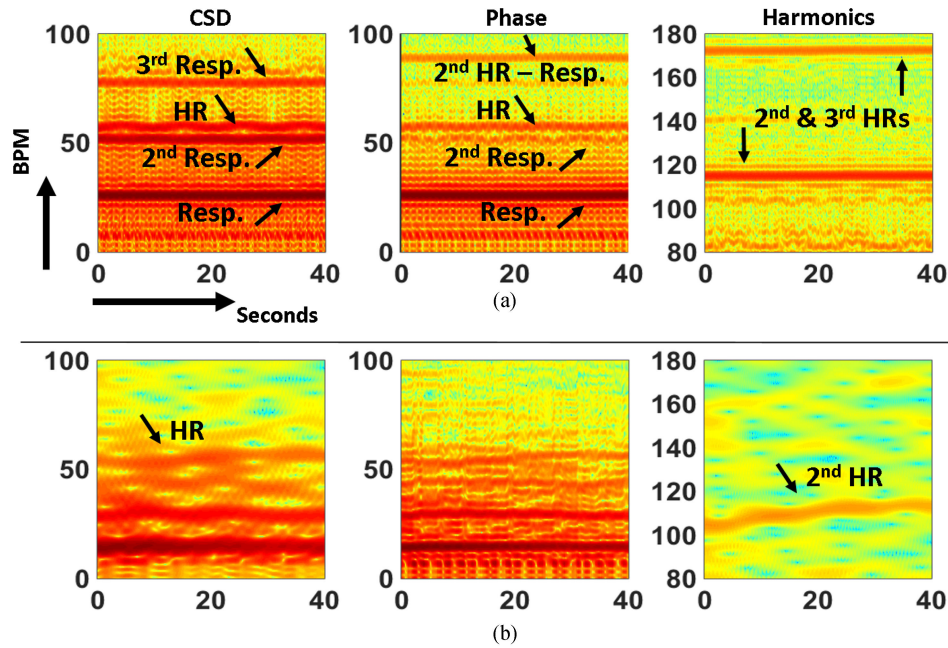
Fig. 9. Time-frequency analysis waterfall plots. (a) Vital signs stimulator. (b) Human subject.

In Fig. 9(a), we can trace the respiration rate and heart rate overtime using CSD, AD methods. However, in the CSD waterfall plot, the heartbeat spectral energy is almost co-located with that of the second-order harmonic of respiration. For the proposed method, the higher-order harmonics second and third are clearly identifiable and, therefore, the heart rate can be estimated correctly. On the other hand, the results from the human subject in Fig. 9(b) show that when the spectrum is noisy around the fundamental heartbeat frequency, it is very difficult to isolate the heartbeat without any previous knowledge, which is the case for the CSD and phased-based waterfall plots in this example. However, in the heartbeat harmonics frequency region, the second-order harmonic of the heartbeat has the most significant spectrum energy over time.

C. Continuous Heart Rate Monitoring Performance Demonstration

The main goal of this paper is to provide a real-time continuous heart rate monitoring algorithm. The analysis in Sections V-A and V-B is from the post-processing perspective and thus the estimates are obtained with the help of visualization and external pulse reference. It should be noted that the phased-based method is not fast enough for real-time processing because of the iterative phase calibration process. For comparison purpose, we record two 2-min data sets and process off-line. We compare three algorithms: the conventional CSD, AD, and the harmonics-based algorithm. The proposed algorithm is strictly implemented following the procedure in Table I.

In Fig. 10, we demonstrate the heart rate monitoring results from the human subjects using two 2-min data sets. In

Fig. 10(a), we compare the continuous heart rate monitoring performance of the proposed method and other popular algorithms. The proposed method provides stable estimates, which gradually changes with time, whereas the results from the other two methods experience huge deviations, which are not physically possible since for stationary subject, we only expect heart rate fluctuate within a few beats.

To be more specific, from 20-s to 78-s, the CSD method has similar performance as that of the proposed method. That is because the respiration rate is relative low at about 14 B/Min and the heart rate is about 58 B/Min. The second-order and third-order harmonics of the respiration is relatively far away from the fundamental heartbeat frequency. Therefore, a bandpass filter is able to separate the fundamental heartbeat and attenuate these respiration harmonics. From about 78-s to 85-s, the human subject starts increasing the respiratory activity to 19 B/Min and maintains at this level until the recording completes. Now the second-order harmonic of respiration is getting closer to the fundamental heartbeat frequency and the third-order harmonics is almost co-located with a fundamental heartbeat frequency. At the respiration acceleration stage (78-s to 85-s), the spectrum region near the fundamental heartbeat frequency becomes noisy, and the fundamental heartbeat frequency peak fades away. The second-order harmonic of heartbeat is the dominant frequency component and therefore the estimate of the CSD method jumps to about 110 B/Min. Once the respiration rate is stable (after 85-s), the spectrum at the relatively lower frequency region becomes less noisy. The second-order harmonic of respiration dominates the spectrum even after the bandpass filter since usually respiration and its harmonics are much stronger
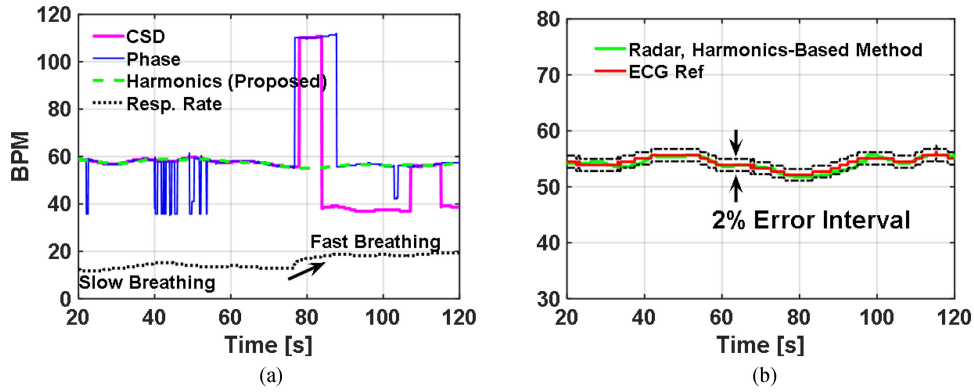
Fig. 10. Continuous heart rate monitoring performance. (a) Robustness against varying breathing tempo. (b) Accuracy demonstration.
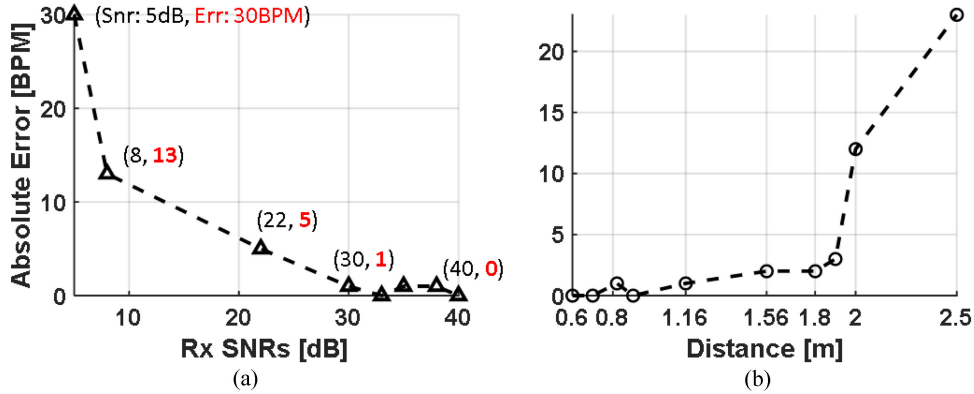

Fig. 11. Heartbeat detection performance demonstration (a) as a function of received signal SNRs and (b) as a function of target distances.

than the heartbeat. As a result, the estimate jumps to the second-order harmonic of respiration at about 38 B/Min. Similar jumps of heart rate estimate occur at 108-s and 115-s for the same reasoning. The AD method performs poorly compared to the other two methods. On top of the overall trend of heart rate, there are lots of fluctuations from the phase-based method. This is an important result, showing that the phased-based method cannot provide consistent estimates. This undesirable result is due to the fact that there is no previous knowledge about which of the I/Q data points need to be corrected. The precise phase calibration procedure is still unknown. Here, the phase calibration is performed on a sliding window of 10-s data and it occasionally introduces phase distortion in the spectrum. That is why the heart rate estimate from the phase-based method (solid blue curve) fluctuates wildly as seen in Fig. 10(a).

In Fig. 10(b), we showcase the accuracy of the proposed heart rate monitoring algorithm by comparing against the gold standard reference ECG sensor. We can see that the heart rate estimates is gradually varying over time. The accuracy is well within 2% error interval about (+/−) 1.1 beats from 20-s to 120-s in data set 2.

D. Limitation Demonstration

In previous results discussion, we have shown that the proposed adaptive method with high integration gain

can provide continuous heart rate measurement with good accuracy at close distance within 1 m. In this section, for completeness, we perform a limitation test on the harmonics-aided heart rate estimation algorithm. To generate Fig. 11(a), eight measurements are taken from a human subject 1 m away from the radar sensor breathing normally. For each measurement, the radar is running at various pulse integration levels. The detection accuracy tends to decrease when the received SNR (or equivalently integration level) is low. The labeled SNRs are estimated from the vital signs spectrum as the ratio of the respiration signal strength to the noise floor. In Fig. 11(b), we use intermediate integration level so the radar scan covers a relatively larger area. In total, ten measurements are taken from 0.5 to 3 m. The corresponding results show that the heart rate detection performance deteriorates with distance. The performance metric is evaluated as the absolute value between the heart rate estimate recovered from the second-order harmonic and the reference pulse rate.

VI. CONCLUSION

In this paper, we presented a new heart rate monitoring algorithm based on a novel concept that estimates the fundamental heart rate from its higher-order features in the spectral domain. We justified the theory through a spectral analysis of the related harmonics. We implemented a

real-time heart rate monitoring system and provided extensive experimental results to demonstrate the effectiveness of the proposed algorithm. For completeness, we also provided discussion on limitations of the proposed algorithm.

ACKNOWLEDGMENT

REFERENCES

[1] J. Li, Z. Zeng, J. Sun, and F. Liu
Through-wall detection of human being's movement by UWB radar
IEEE Geosci. Remote Sens. Lett., vol. 9, no. 6, pp. 1079–1083, Nov. 2012.

[2] Y. Wang, Q. Liu, and A. E. Fathy
CW and pulse–doppler radar processing based on FPGA for human sensing applications
IEEE Trans. Geosci. Remote Sens., vol. 51, no. 5, pp. 3097–3107, May 2013.

[3] V.-H. Nguyen and J.-Y. Pyun
Location detection and tracking of moving targets by a 2D IR-UWB radar system
Sensors, vol. 15, no. 3, pp. 6740–6762, 2015.

[4] E. M. Staderini
UWB radars in medicine
IEEE Aerosp. Electron. Syst. Mag., vol. 17, no. 1, pp. 13–18, Jan. 2002.

[5] C.-P. Lai, R. Narayanan, Q. Ruan, and A. Davydov
Hilbert–Huang transform analysis of human activities using through-wall noise and noise-like radar
IET Radar, Sonar Navig., vol. 2, no. 4, pp. 244–255, 2008.

[6] J. W. Choi, D. H. Yim, and S. H. Cho
People counting based on an IR-UWB radar sensor
IEEE Sensors J., vol. 17, no. 17, pp. 5717–5727, Sep. 2017.

[7] M. G. Hussain
Ultra-wideband impulse radar-An overview of the principles
IEEE Aerosp. Electron. Syst. Mag., vol. 13, no. 9, pp. 9–14, Sep. 1998.

[8] C. G. Bilich
Bio-medical sensing using ultra wideband communications and radar technology: A feasibility study
In *Proc. Pervasive Health Conf. Workshops*, 2006, pp. 1–9.

[9] R. Chavez-Santiago, I. Balasingham, and J. Bergsland
Ultrawideband technology in medicine: A survey
J. Electr. Comput. Eng., vol. 2012, 2012, Art. no. 716973.

[10] C. Li and J. Lin
Complex signal demodulation and random body movement cancellation techniques for non-contact vital sign detection
In *Proc. IEEE MTT-S Int. Microw. Symp. Dig.*, 2008, pp. 567–570.

[11] B.-K. Park, O. Boric-Lubecke, and V. M. Lubecke
Arctangent demodulation with DC offset compensation in quadrature doppler radar receiver systems
IEEE Trans. Microw. Theory Techn., vol. 55, no. 5, pp. 1073–1079, May 2007.

[12] J. Wang, X. Wang, L. Chen, J. Huangfu, C. Li, and L. Ran
Noncontact distance and amplitude-independent vibration measurement based on an extended DACM algorithm
IEEE Trans. Instrum. Meas., vol. 63, no. 1, pp. 145–153, Jan. 2014.

[13] A. Lazaro, D. Girbau, and R. Villarino
Analysis of vital signs monitoring using an IR-UWB radar
Progress Electromagn. Res., vol. 100, pp. 265–284, 2010.

[14] L. Ren, Y. S. Koo, Y. Wang, and A. E. Fathy
Noncontact heartbeat detection using UWB impulse doppler radar
In *Proc. IEEE Topical Conf. Biomed. Wireless Technol., Netw., Sens. Syst.*, 2015, pp. 1–3.

[15] Y. Rong and D. W. Bliss
Direct RF signal processing for heart-rate monitoring using UWB impulse radar
In *Proc. 52nd Asilomar Conf. Signals, Syst., Comput.*, 2018, pp. 1215–1219.

[16] L. Ren, H. Wang, K. Naishadham, O. Kilic, and A. E. Fathy
Phase-based methods for heart rate detection using UWB impulse doppler radar
IEEE Trans. Microw. Theory Techn., vol. 64, no. 10, pp. 3319–3331, Oct. 2016.

[17] Y. Rong and D. W. Bliss
Harmonics-based multiple heartbeat detection at equal distance using UWB impulse radar
In *Proc. IEEE Radar Conf.*, 2018, pp. 1101–1105.

[18] Y. Rong and D. W. Bliss
Smart homes: See multiple-heartbeats through wall using wireless signals
In *Proc. IEEE Radar Conf.*, 2019.

[19] L. Ren, Y. S. Koo, H. Wang, Y. Wang, Q. Liu, and A. E. Fathy
Noncontact multiple heartbeats detection and subject localization using UWB impulse doppler radar
IEEE Microw. Wireless Compon. Lett., vol. 25, no. 10, pp. 690–692, Oct. 2015.

[20] N. Chernov and C. Lesort
Least squares fitting of circles
J. Math. Imag. Vis., vol. 23, no. 3, pp. 239–252, 2005.

[21] M. Zakrzewski, H. Raittinen, and J. Vanhala
Comparison of center estimation algorithms for heart and respiration monitoring with microwave doppler radar
IEEE Sensors J., vol. 12, no. 3, pp. 627–634, Mar. 2012.

[22] A. Singh *et al.*
Data-based quadrature imbalance compensation for a CW doppler radar system
IEEE Trans. Microw. Theory Techn., vol. 61, no. 4, pp. 1718–1724, Apr. 2013.

[23] S. Guan, J. A. Rice, C. Li, and C. Gu
Automated dc offset calibration strategy for structural health monitoring based on portable cw radar sensor
IEEE Trans. Instrum. Meas., vol. 63, no. 12, pp. 3111–3118, Dec. 2014.

[24] *Emergency Care for You: ER 101*. American College of Emergency Physicians Foundation, 2014.

[25] M. Singh and G. Ramachandran
Reconstruction of sequential cardiac in-plane displacement patterns on the chest wall by laser speckle interferometry
IEEE Trans. Biomed. Eng., vol. 38, no. 5, pp. 483–489, May 1991.

[26] N. Andersen *et al.*
A 118-MW pulse-based radar SOC in 55-nm CMOS for non-contact human vital signs detection
IEEE J. Solid-State Circuits, vol. 52, no. 12, pp. 3421–3433, Dec. 2017.

Yu Rong (S'17) received the B.S. degree from the University of Chengdu Information Technology, Chengdu, China, in 2010, and the M.S. degree from the University of Maryland, College Park, MD, USA, in 2012. He is currently working toward the Ph.D. degree in electrical engineering with Arizona State University, Tempe, AZ, USA.

He joined Bliss Laboratory Information of Signals and Systems, Arizona State University in 2013.

Daniel W. Bliss (F'15) received the B.S. degree in electrical engineering from Arizona State University (ASU), Tempe, AZ, USA, in 1989, and the M.S. and Ph.D. degrees in physics from the University of California at San Diego, La Jolla, CA, USA, in 1995 and 1997.

He is the Director of the Center for Wireless Information Systems and Computational Architectures, ASU. He is an Associate Professor with the School of Electrical, Computer, and Energy Engineering, ASU. He is responsible for foundational work in electronic protection, adaptive multiple-input multiple-output (MIMO) communications, MIMO radar, distributed-coherent systems, and RF convergence. Before moving to ASU, he was a Senior Member of the Technical Staff with MIT Lincoln Laboratory (1997–2012). He has also made significant contributions to medical and physiological analytics. Between his undergraduate and graduate degrees, he was employed with General Dynamics (1989–1993), where he designed avionics for the Atlas-Centaur launch vehicle, and performed magnetic field optimization for high-energy particle-accelerator superconducting magnets. His doctoral work (1993–1997) was in the area of high-energy particle physics and lattice-gauge-theory calculations. He has published more than 100 technical articles and conference papers. His current research interests include advanced systems in the areas of communications, radar, precision positioning, and medical monitoring. To achieve these goals, he develops and employs information, detection, and estimation theory, and algorithm development, including machine learning.